Simulation of Semiconductor Processes and Devices 2016
Edited by E. Bär, J. Lorenz, and P. Pichler

Multi-Subband Ensemble Monte Carlo Study of Band-to-Band Tunneling in Silicon-based TFETs

C. Medina-Bailon*†, C. Sampedro*, J.L. Padilla*, F. Gamiz*, A. Godoy* and L. Donetti*

* Nanoelectronics Research Group, Universidad de Granada, 18071 Granada, Spain.

†e-mail: cmedba@ugr.es

***Abstract*—TFETs have become an alternative to conventional MOSFETs in the last years due to the possibility of achieving low subthreshold swing (SS) that allows for low off current and operation at low V_{DD}. In this work a non-local band-to-band tunneling model has been successfully implemented into a Multi-Subband Ensemble Monte Carlo (MS-EMC) simulator and applied to ultra-scaled silicon-based n-type TFETs. Different approaches for the choice of the tunneling path have been compared and relevant differences are observed in both the current levels and the spatial distribution of the generated carriers.**

I. Introduction

In the last decades, different alternative technologies and materials have been studied to replace the conventional MOSFETs and to extend the end of the roadmap [1]. One of the main trends seeks the exploitation of new transport mechanisms and physical phenomena taking advantage from new materials and nanometric dimensions. The tunnel field-effect transistor (TFET) is one of the devices proposed to reach sub-60 mV/dec subthreshold swing (SS) [2]. The most important difference between both architectures is the injection mechanism which in conventional MOSFETs is governed by the thermionic emission above the source barrier, whereas in TFETs the carrier injection mechanism is replaced by quantum mechanical tunneling through the barrier (band-to-band tunneling (BTBT)). This work presents the development and implementation of BTBT model in a Multi-Subband Ensemble Monte Carlo (MS-EMC) simulator and its application to the study of ultra-scaled silicon-based n-type TFETs. Furthermore, the impact of different tunneling path choices on the generation rate has been elucidated in our work.

II. Simulation Set-up

The starting point of the simulation frame is a MS-EMC code which has already demonstrated its capabilities in different scenarios [3]–[5] keeping a reasonable computational effort with respect to the full-quantum approach. The tool is based on the mode-space approach of quantum transport [6] where the system is decoupled in the confinement direction and the transport plane, where the 1D Schrödinger equation and the 2D Boltzmann Transport Equation (BTE) are solved, respectively (Figure 1). Both equations are coupled to the 2D Poisson Equation to keep the self-consistency of the solution. Moreover, quantum transport effects can be included in a separate way because of the decoupled approximation [7], [8].

978–1–5090–0818–6/16/$31.00 ©2016 IEEE

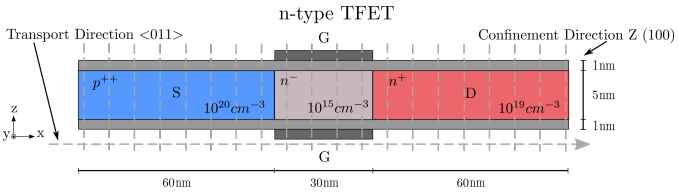

Fig. 1: Silicon-based n-type TFET structure analyzed in this work. 1D Schrödinger equation is solved for each grid point in the transport direction and BTE is solved by the MC method in the transport plane.

The simulated silicon-based n-type TFET is schematically presented in Figure 1, as well as doping concentrations and device parameters. The center of the device in x direction corresponds to $x = 0nm$. An n-type doped drain concentration of $N_D = 10^{19}cm^{-3}$, a p-type doped source concentration $N_S = 10^{20}cm^{-3}$, an n-doped channel of $10^{15}cm^{-3}$ with a $30nm$ channel length, channel thickness $T_{Si} = 5nm$, a gate oxide of SiO_2 with Equivalent Oxide Thickness $EOT = 1nm$, and gate work function of $4.05eV$ are considered in the simulations.

The algorithm developed in this study implements the non-local direct and phonon assisted BTBT considering quantum confinement effects through discretization of conduction and valence bands into energy subbands. Figure 2 depicts the flowchart of the modified MS-EMC simulator where the additional blocks are represented. The spatial variation of the energy bands has been taken into account for implementing BTBT thanks to the non-local model, so that the tunneling process can be more accurately described. The semiclassical model herein developed translates the tunneling current into suitable generation rates (G_{BTBT}) for electrons in the conduction band and for holes in valence band. This simplifies the treatment of the BTBT and allows low computational cost. Moreover, these blocks can be calculated at a different time step than the Monte Carlo loop allowing a better optimization of the computational load.

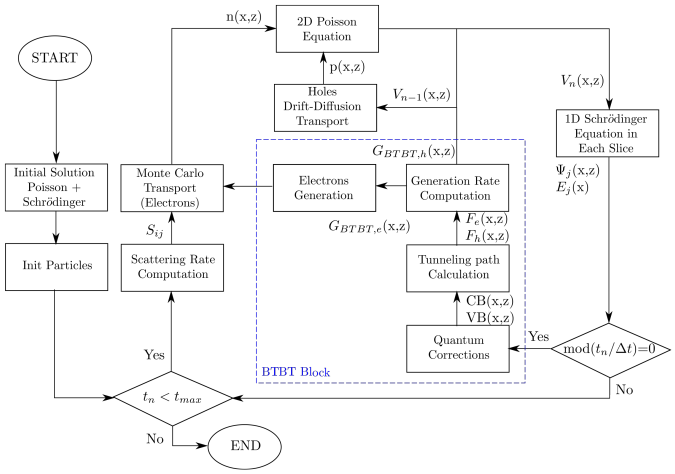

Fig. 2: Flowchart of the MS-EMC simulator with the additional blocks of the BTBT code where x is the transport direction, z the confinement direction, $n(x,z)$ and $p(x,z)$ are the electron and hole concentrations, respectively, $V(x,z)$ is the potential profile, $E_j(x)$ is the subband energy, $\Psi_j(x,z)$ are the subband eigenfunctions, S_{ij} are the scattering rates, subscript n stands for the iteration number, Δt is the time step where BTBT is calculated, $F_e(x,z)$ and $F_h(x,z)$ are the electric field of electrons and holes associated to the selected tunneling path, and $G_{BTBT,e}(x,z)$ and $G_{BTBT,h}(x,z)$ are the electron and hole generation rates, respectively.

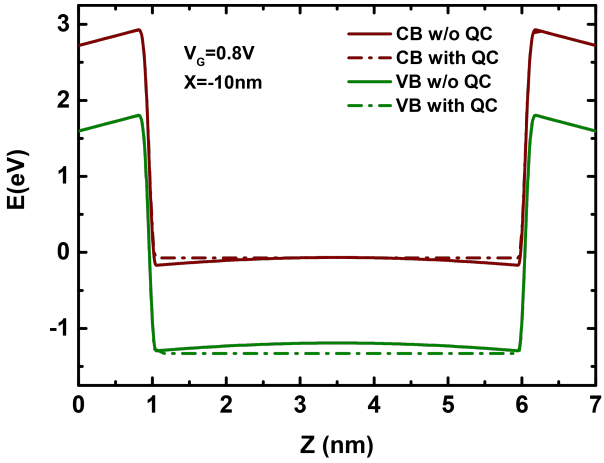

Fig. 3: Quantum corrections included in the conduction and valence bands for $V_{GS} = 0.8V$, $V_{DS} = 1V$ and $x = -10nm$ being $x = 0nm$ the center of the device in x direction.

The first block in this model corresponds to the quantum corrections for the conduction and valence bands. In MS-EMC simulators the carriers are placed into subbands and, at given x, their position distribution in z is set by the solution of the Schrödinger Equation. Thus, a mapping procedure between 2D conduction and valence bands and their respective subbands is required. If this correction is not considered, the generated particles by BTBT can reach a location whose energy is lower (resp. higher) than that corresponding to the first subband in the conduction band (resp. valence band). This procedure would imply a violation of the energy conservation principle and would therefore result into significant errors. It is hence necessary to include a band profile modification to account for quantization, which is depicted in Figure 3. Let us now describe the procedure to do so. In the conduction band, given that the first subband is known ($E_0^c(x)$), for all points verifying $E_c(x,z) \leq E_0^c(x)$, we set $E_c(x,z) = E_0^c(x)$. As for the valence band, since holes are mainly generated in the source, its profile can be accurately approximated along z by a rectangular well. Therefore, for all points where $E_v(x,z) \geq E_0^v(x)$ we set $E_v(x,z) = E_0^v(x)$ provided that $E_0^v(x)$ is the first hole eigenvalue resulting from the analytical resolution of the rectangular well profile:

$$E_0^v(x) = E_{v,max}(x) - \frac{1}{2m_h^*}\left(\frac{\pi\hbar}{T_{si}}\right) \quad (1)$$

Two different BTBT path assumptions have been included in the tunneling calculation block [9]. The first one computes the path following the valence band maximum gradient trajectory (F_{max}). In this case, the tunneling path changes dynamically depending on the self-consistent potential computed during the simulation. According to this, so does the generation rate changes dynamically with the device bias because the direction of the tunneling path is modified by the electrostatic configuration. The second one considers a "minimum length" tunneling path (L_{min}). The choice of F_{max} could be the most realistic and reasonable tunneling path because the electrons tunnel following the direction imposed by the electric field. However, the carriers can tunnel in many directions which means that L_{min} could be also a valid assumption. For both assumptions, a maximum tunneling rejection length is also introduced (L_{max}) to consider a realistic tunneling path. In this work, L_{max} has been chosen according to the channel length dimensions, $L_{max} = L_G = 30nm$.

In this BTBT block, the tunneling path choice gives rise to an average electric field of electrons ($F_e(x,z)$) and another one for holes ($F_h(x,z)$). At this point, it is necessary to emphasize that these electric fields are different from each other because both types of particles undergo independent paths. That is to say, the generated electrons can reach the same ending point in the conduction band, whereas the corresponding holes can be generated at different starting points in the valence band. The tunneling rate is therefore not anymore solely dependent on the local electric field at the starting point, but also on the full tunneling barrier profile and on the selected tunneling path.

The next step is to calculate the generation rates for electrons and holes. This algorithm is based on the Kane's model to determine the BTBT generation rate G_{BTBT} per unit of volume [10], [11]:

$$G_{BTBT,e}(x,z) = A\left(\frac{F_e(x,z)}{F_0}\right)^P \exp\left(-\frac{B}{F_e(x,z)}\right) \quad (2)$$

$$G_{BTBT,h}(x,z) = A\left(\frac{F_h(x,z)}{F_0}\right)^P \exp\left(-\frac{B}{F_h(x,z)}\right) \quad (3)$$

where F_0=1V/m, P=2.5 for the phonon assisted tunneling process, and F is the electric field. In addition, the prefactor A and the exponential factor B that account for indirect transitions are expressed as follows:

$$A = \frac{g\,(m_v m_c)^{3/2}\,(1+2N_{TA})\,D_{TA}^2\,(qF_0)^{5/2}}{2^{21/4}h^{5/2}m_r^{5/4}\rho\epsilon_{TA}\left[E_g(300K)+\Delta_c\right]^{7/4}} \quad (4)$$

$$B = \frac{2^{7/2}\pi m_r^{1/2}\left[E_g(300K)+\Delta_c\right]^{3/2}}{3qh} \quad (5)$$

where g is a degeneracy factor, m_c and m_v are the conduction and valence band density of states effective masses, respectively, m_r is the reduced tunneling mass, N_{TA} is the occupation number of the transverse acoustic phonons at temperature T, D_{TA} is the deformation potential of transverse acoustic phonons, and ϵ_{TA} is the transverse acoustic phonon energy. The rest of the parameters takes their usual meaning. Only the transverse acoustic phonons are taken into account because they have the highest phonon occupation number and the smallest phonon energy.

Most of the BTBT models available in the literature are one-dimensional [12], [13]. The common approach adopted in TCAD simulation is to perform the tunneling calculation along several one-dimensional paths chosen to lay along the direction of the maximum electric field. The BTBT code described above presents the advantage of calculating the two-dimensional tunneling path dynamically at each simulation step accordingly to the up-to-date electrostatic configuration.

After the calculation of G_{BTBT} and the tunneling path, it is necessary to include the generated charge in a self-consistent way [14]. On the one hand, since holes travel mostly in the low field source region, they are not treated as individual particles and a drift diffusion approach is used to describe them. For this reason, the hole concentration is corrected from the hole generation rate at each time step ($\Delta p_{BTBT}(x,z) = G_{BTBT,h}(x,z)\cdot\Delta t$) following Scharfetter-Gummel discretization scheme [15]. On the other hand, a number of superparticles representing electrons, N_e, are generated in the BTBT process which depends on the time step, Δt, the statistical weight, w, and the electron generation rate $G_{BTBT,e}(x,z)$ at the position of the superparticle, x_i. Firstly, these superparticles are generated in the fundamental subband with x_i chosen randomly inside the considered grid cell with a probability distribution given by P(x) due to the 2D MS-EMC approximation:

$$P(x) = \frac{\int_0^{T_{Si}} G_{BTBT,e}(x,z)\,dz}{\int\int_0^{T_{Si}} G_{BTBT,e}(x,z)\,dx\,dz} \quad (6)$$

Secondly, the number of particles is calculated taking into account the equivalent generation rate in the considered slice x_i:

$$N_e = \frac{\Delta T}{w}\int_0^{T_{Si}} G_{BTBT,e}(x_i,z)\,dz \quad (7)$$

III. Results and Discussion

The inclusion of this effect has an important impact on $I_D - V_{GS}$ characteristics for both tunneling path assumptions as depicted in Figure 4. However, the resulting ON current level (I_{ON}) proves to be very low in this silicon-based TFETs due to its large indirect energy band gap. Some significant facts can be pointed out from Figure 4: the current level predicted by the L_{min} trajectory results in a significantly smaller current level in the subthreshold regime along with a steeper slope compared to the F_{max} approach. In addition, the current obtained for L_{min} is non-monotonous.

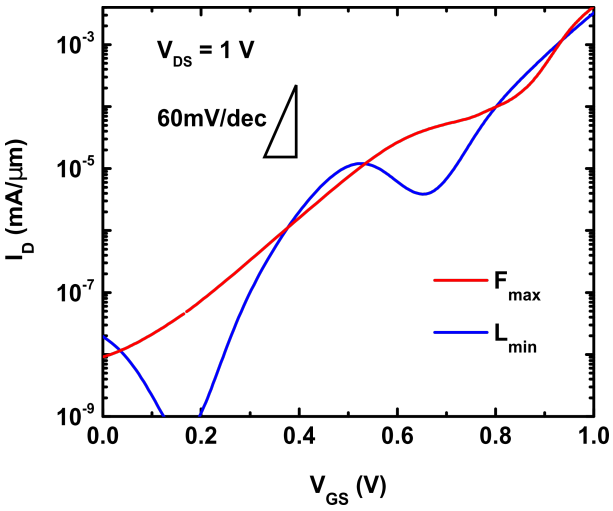

Fig. 4: I_{DS} vs. V_{GS} at saturation regime for both tunneling path assumptions: the tunneling path following the valence band maximum gradient trajectory (F_{max}), and the minimum length tunneling path (L_{min}).

The number of particles generated is also affected by the tunneling path assumption as shown in Figure 5. These particles in the on state when the shortest tunneling path assumption is considered are higher than those obtained when the particles follow the direction of the maximum valence band gradient. This effect is also plotted in Figure 6 where the population of the first subband is represented as a function of the total energy.

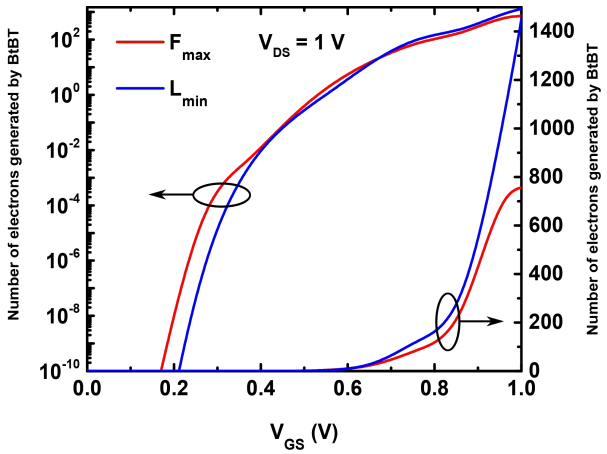

Fig. 5: Number of electrons generated by BTBT for both tunneling path assumptions: the tunneling path following the valence band maximum gradient trajectory (F_{max}), and the minimum length tunneling path (L_{min}). For the sake of clarity log and linear scales are shown on the left and right axes, respectively.

IV. Conclusions

This work presents the implementation of a novel BTBT block in a MSB-EMC tool for the study of ultra-scaled silicon-based n-type TFETs allowing a detailed scattering description and a moderate computational cost. Two different tunneling path assumptions have been analyzed, L_{min} and F_{max}. Further developments will be required to include direct band gap material devices to obtain higher I_{ON}.

V. Acknowledgment

The authors are grateful for the support given by the Spanish Ministry of Science and Innovation (TEC2014-59730-R), H2020 - REMINDER (687931), H2020 - WAYTOGO-FAST (662175), and Marie Curie Action through the Programme Andalucia Talent Hub (291780).

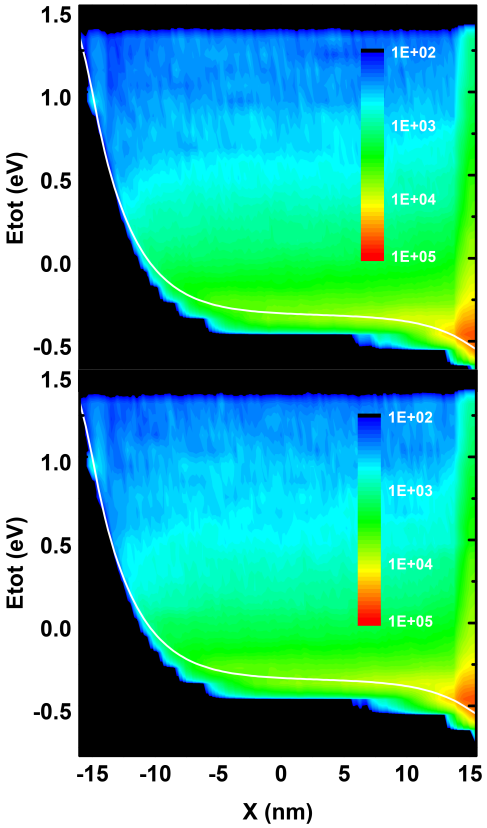

Fig. 6: Electron distribution as a function of total energy including BTBT for both tunneling path assumptions: the tunneling path following the valence band maximum gradient trajectory (top), and the minimum length tunneling path (bottom). Both cases correspond to $V_{GS} = 0.8V$ and $V_{DS} = 1V$.

References

[1] H.-S. Wong, "Beyond the conventional transistor," *IBM Journal of Research and Development*, vol. 46, pp. 133–168, March 2002.

[2] A. Ionescu and H. Riel, "Tunnel field-effect transistors as energy-efficient electronic switches," *Nature*, vol. 479, pp. 329–337, November 2011.

[3] C. Sampedro, F. Gámiz, A. Godoy, R. Valín, A. García-Loureiro, N. Rodríguez, I. M. Tienda-Luna, F. Martinez-Carricondo, and B. Biel, "Multi-Subband Ensemble Monte Carlo simulation of bulk MOSFETs for the 32 nm-node and beyond," *Solid-State Electronics*, vol. 65-66, no. 1, pp. 88–93, 2011.

[4] C. Sampedro, F. Gámiz, L. Donetti, and A. Godoy, "Reaching sub-32 nm nodes: ET-FDSOI and BOX optimization," *Solid-State Electronics*, vol. 70, pp. 101–105, 2012.

[5] C. Sampedro, F. Gámiz, and A. Godoy, "On the extension of ET-FDSOI roadmap for 22 nm node and beyond," *Solid-State Electronics*, vol. 90, pp. 23–27, 2013.

[6] R. Venugopal, Z. Ren, S. Datta, M. S. Lundstrom, and D. Jovanovic, "Simulating quantum transport in nanoscale transistors: Real versus mode-space approaches," *Journal of Applied Physics*, vol. 92, no. 7, pp. 3730–3739, 2002.

[7] C. Medina-Bailon, C. Sampedro, F. Gámiz, A. Godoy, and L. Donetti, "Impact of S / D Tunneling in Ultrascaled Devices, a Multi-Subband Ensemble Monte Carlo Study." 2015 International Conference on Simulation of Semiconductor Processes and Devices (SISPAD), 2015, pp. 21–24.

[8] ——, "Confinement orientation effects in S / D tunneling." 2016 Joint International EUROSOI Workshop and International Conference on Ultimate Integration on Silicon (EUROSOI-ULIS), 2016, pp. 100–103.

[9] L. De Michielis, M. Iellina, P. Palestri, A. M. Ionescu, and L. Selmi, "Effect of the choice of the tunnelling path on semi-classical numerical simulations of TFET devices," *Solid-State Electronics*, vol. 71, pp. 7–12, May 2012.

[10] E. O. Kane, "Theory of Tunneling," *Journal of Applied Physics*, vol. 32, no. 1, p. 83, 1961.

[11] W. Vandenberghe, B. Sorée, W. Magnus, and M. V. Fischetti, "Generalized phonon-assisted Zener tunneling in indirect semiconductors with non-uniform electric fields: A rigorous approach," *Journal of Applied Physics*, vol. 109, no. 12, p. 124503, 2011.

[12] Synopsys, "Sentaurus Device User Version 2014.09," no. September, 2014.

[13] K.-h. Kao, S. Member, A. S. Verhulst, W. G. Vandenberghe, S. Member, B. Sorée, G. Groeseneken, and K. D. Meyer, "Direct and Indirect Band-to-Band Tunneling in Germanium-Based TFETs," vol. 59, no. 2, pp. 292–301, 2012.

[14] A. Revelant, P. Palestri, and L. Selmi, "Multi-subband semi-classical simulation of n-type Tunnel-FETs," *2012 13th International Conference on Ultimate Integration on Silicon (ULIS)*, pp. 187–190, Mar. 2012.

[15] S. Selberherr, *Analysis and Simulation of Semiconductor Devices*. New York: Springer-Verlag, 1984.